

Colloidal Gelation with Non-Sticky Particles

Yujie Jiang^{1,2,*} and Ryohei Seto^{1,3,4,†}

¹Wenzhou Key Laboratory of Biomaterials and Engineering, Wenzhou Institute, University of Chinese Academy of Sciences, Wenzhou, Zhejiang 325000, China

²School of Physical Sciences, University of Chinese Academy of Sciences, Beijing 100049, China

³Oujiang Laboratory (Zhejiang Lab for Regenerative Medicine, Vision and Brain Health), Wenzhou, Zhejiang 325000, China

⁴Graduate School of Information Science, University of Hyogo, Kobe, Hyogo 650-0047, Japan

(Dated: June 12, 2025)

Colloidal gels are widely applied in industry due to their rheological character—no flow takes place below the yield stress. Such property enables gels to maintain uniform distribution in practical formulations; otherwise, solid components may quickly sediment without the support of gel matrix. Compared with pure gels of sticky colloids, therefore, the composites of gel and non-sticky inclusions are more commonly encountered in reality. Through numerical simulations, we investigate the gelation process in such binary composites. We find that the non-sticky particles not only confine gelation in the form of an effective volume fraction, but also introduce another lengthscale that competes with the size of growing clusters in gel. The ratio of two key lengthscales in general controls the two effects. Using different gel models, we verify such scenario within a wide range of parameter space, suggesting a potential universality in all classes of colloidal composites.

INTRODUCTION

Sticky colloidal particles diffuse and aggregate into clusters until forming a ramified, space-spanning network, i.e., colloidal gel [1, 2]. Due to the load-bearing structure, colloidal gels behave as soft solids with finite yield stress beyond which flow occurs [3, 4]. This rheological signature enables gels to be widely applied in industry, ranging from foodstuffs and personal care products to pharmaceuticals and biotechnology [5–7]. Through experiments and simulations, particulate gels of monodisperse attractive (i.e., single-component) colloids have been extensively studied in various aspects (e.g., structure [2], dynamics [5] and rheology [8]), while theories have been proposed to approach *a priori* prediction (such as [9]). By contrast, realistic gel-like materials, which usually contain multiple components, remain less probed. This is partially due to the lack of proper model systems in experiments, while the intrinsic complication of polydispersity also limits the progress in fundamental understanding. While recent attention on composite systems increases [10–15], most studies still remain on the phenomenological level of *ac hoc* models.

Among the diverse array of multi-component systems, the combination of gel matrix and solid fillers is prototypical in practical applications. For example, polymeric nanocomposites have remarkable mechanical properties and are ubiquitous in sensors, civil engineering, and microbial applications [16]. Progress has been made in understanding such composites, which, in the absence of strong filler–matrix interactions, can be described by conventional continuum mechanics [17]. Because of a large gap between the constituent sizes, empirical approaches (such as Krieger–Dougherty law) have been found to describe the basic behavior by assuming a continuum back-

ground [18, 19].

However, the continuum assumption no longer holds if the characteristic sizes of each component are comparable [20]. This is the case when replacing the polymer matrix in polymeric nanocomposites with a colloidal gel network, where the typical lengthscales are all micron-sized. The interplay between these lengthscales generates novelty. Though not yet fully understood, such biphasic mixtures receive increasing attention [21, 22], and recent work reports a unique flow-switched bistability [23], which has never been observed in regular gels. These observations suggest the essential role of filler (or inclusion [17]) particles. While researchers have recently focused on the gelled state of these composites [17, 24], the inclusion effect on gelation dynamics is still unclear.

Using numerical simulations, we aim to shed light on the understanding of colloidal gelation with non-sticky particle fillers. The system we investigate is composed of sticky colloids, which can form a percolating gel network on their own, and non-sticky (NS) particles, which are hard spheres. As the latter stick neither to the gel colloids nor to themselves, they do not participate in gelation directly. Then the intuitive assumption seems to view NS particles as a confinement to the gel part by compressing the available volume. Through extensive exploration of the parameter space, we show that the interplay between comparable lengthscales also plays a vital role and, in some cases, dominates over the confining effect and greatly impedes the gelation process. The ratio of two key lengthscales, i.e., the characteristic size of gel and the NS-particle spacing, offers a robust measure for such interplay, which controls the cluster growth during gelation. We verify this scenario over a wide range of compositions and particle sizes in different types of colloidal gel.

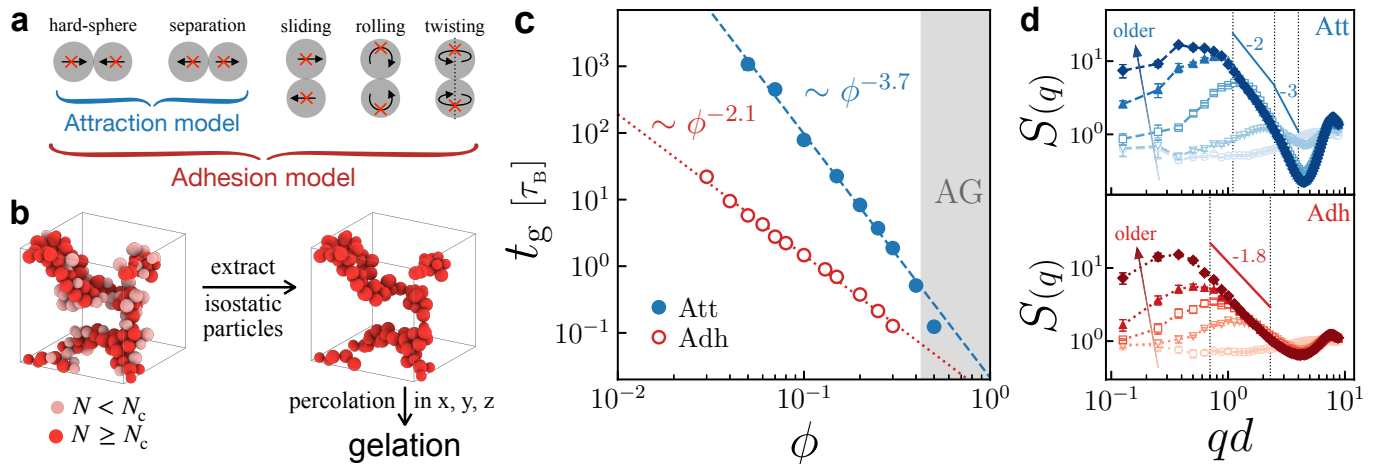


Fig. 1. Gelation dynamics of colloidal gels. **a** Sketches of possible pairwise motions and two contact models with constraints shown in red crosses. **b** Schematic gelation determination. See details in the Methods section. **c** Gelation times t_g as functions of volume fraction ϕ in different gels. The blue dashed line and red dotted line are power-law fittings with results shown in Eqs. (1) and (2). Gray region denotes attractive glass (AG) regime. **d** Evolution of structure factors $S(q)$ in an attractive gel ($\phi = 0.1$, top) and an adhesive gel ($\phi = 0.05$, bottom). The open and filled symbols represent $S(q)$ of snapshots before and upon gelation, respectively, and the arrows indicate time evolutions (from bottom to top: $t/\tau_B = 0, 1, 10, 100$, and 1000). Solid lines indicate the slope at intermediate wavenumbers.

RESULTS

Colloidal gelation. A variety of attractions lead to colloidal gelation in nature, such as van der Waals forces, depletion forces, and hydrophobic interactions [25]. In this work, we investigate gelation under strong attractions ($U_{\text{att}} \gg k_B T$) within a wide range of volume fractions ($0.03 \leq \phi \leq 0.3$). We consider two typical contact models. The first model refers to typical attractions which drive particles to aggregate with only radial forces, as shown in Fig. 1 a (blue). Such conservative attractions are characterized by pairwise potentials and mostly apply to smooth particles [2] without tangential constraints, i.e., particles in contact can freely slide and rotate. By contrast, the second model constrains tangential pairwise motions (sliding, rolling, twisting) with the presence of attraction, Fig. 1 a (red). As suggested in [26], we term the first contact as attraction (att) and the second model with tangential constraints as adhesion (adh).

The difference in contact interactions leads to different micromechanics, such as bending rigidity [27] and isostaticity [28]. Based on the Maxwell criteria [29], mechanical stability for frictionless particles in 3D requires an average contact number $N \geq N_c = 6$. Following [30], we consider the isostaticity condition as microstructural information in attractive and adhesive systems and determine gelation accordingly. In particular, we extract particles with $N \geq N_c$ and check their connectivity (see the Methods section), Fig. 1 b. The gelation point determined by this method has been verified, in both experiments [31] and simulations [24], to agree well with that from macroscopic rheology. Therefore, we apply this

gelation criterion throughout this work, with $N_c^{\text{att}} = 6$ for attractive gels and $N_c^{\text{adh}} = 2$ for adhesive gels [28].

Our simulations start from a random, homogeneous configuration and evolves following Langevin dynamics for up to 10^4 Brownian time $\tau_B \equiv \pi\eta d^3/2k_B T$ (where η refers to fluid viscosity and d to colloid diameter). More simulation details can be found in the Methods section. For both gels, the time required for gelation t_g decreases with the volume fraction ϕ in a power-law manner, Fig. 1 c. Fitting of attractive gel data (blue) gives an exponent of -3.7 , while that of adhesive gels (red) exhibits a lower exponent -2.1 . Detailed fitting results are as follow:

$$t_g^{\text{att}} \approx 0.021 \times \phi^{-3.7}, \quad (1)$$

$$t_g^{\text{adh}} \approx 0.011 \times \phi^{-2.1}. \quad (2)$$

At the same volume fraction ϕ , it takes adhesive colloids less time to gel than the attractive ones. The exponents roughly agree with the values in other literature [32–34], justifying our gel simulations as well as the gelation criterion we used.

To capture the structural evolution during gelation, we measure the static structure factor $S(q)$ for both attractive ($\phi = 0.1$) and adhesive ($\phi = 0.05$) gels, Fig. 1 d. $S(q)$ is originally flat due to the homogeneous randomization for the initial configuration. As time increases (indicated by arrows in Fig. 1 d), a peak at intermediate wavenumber q appears, grows, and shifts to a lower q . Thus, a characteristic lengthscale $\xi \equiv 2\pi/q_0$ (where q_0 refers to the peak position) increases during gelation, plausibly representing the cluster growth. Note that the low- q

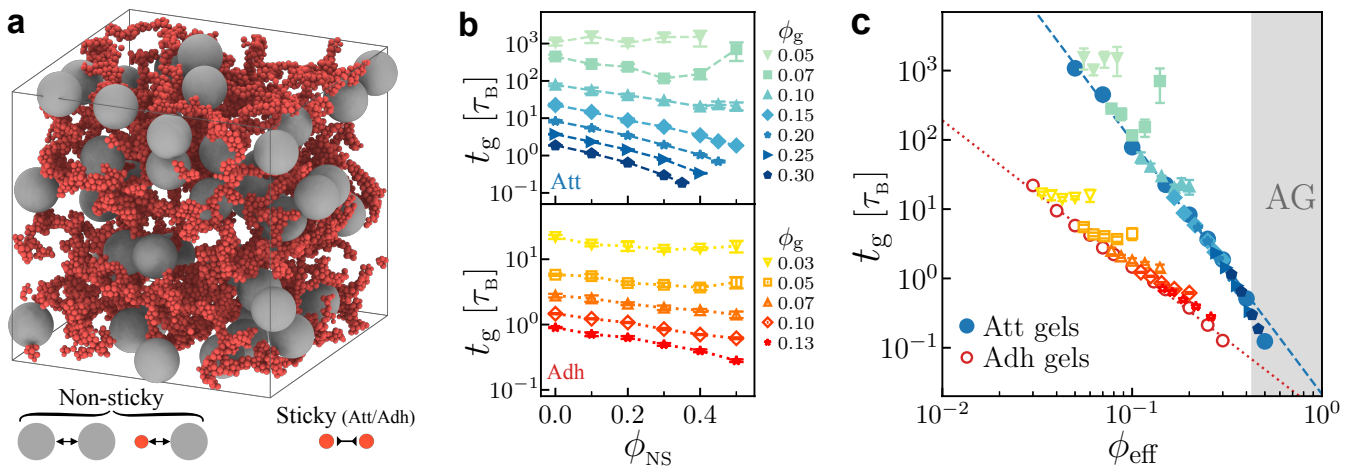


Fig. 2. Colloidal gelation with non-sticky particles. **a** 3D rendering of a gelled attractive system of $d_{NS} = 8d$ at $\phi_g = 0.05$ and $\phi_{NS} = 0.1$. Red and gray spheres represent sticky colloids and non-sticky particles, respectively. **b** Gelation times t_g of attractive (top) and adhesive (bottom) systems of $d_{NS} = 8d$ vary as functions of ϕ_{NS} at different ϕ_g . Data with $\phi_{NS} = 0$ refer to colloidal gels. **c** Plot of the same data in **b** with t_g versus ϕ_{eff} (defined in Eq. (3)). The dashed blue line and dotted red line are the power-law fittings of gel data in Fig. 1 b, also see Eqs. (1) and (2).

peak is absent at $\phi = 0.5$ (Supplementary Note 1), indicating a homogeneous attractive glass (AG) state. The gel-to-glass transition explains the slight deviation from the power-law scaling of t_g , Fig. 1 c (blue).

While the two systems exhibit similar $S(q)$ evolutions, the fractal dimensions d_f inside clusters, which can be estimated from the slope of $S(q) \sim q^{-d_f}$ [35], are different. According to Fig. 1 d (top), the clusters in attractive gel are rather compact ($d_f \approx 3$) at short range, suggesting gelation via the typical arrested-phase-separation route [2, 25]. As q decreases, the fractal dimension d_f drops to 2 (consistent with the value reported in [7]), indicating a relatively open structure at larger length-scales. We attribute this to the emergent bending rigidity of bigger building blocks, e.g., tetrahedrons composed of attractive particles.

By contrast, the gel network in the adhesive gel is more open and ramified with a lower fractal dimension $d_f \approx 1.8$, as expected by diffusion-limited cluster-cluster aggregation (DLCA) [25]. Since the clusters in adhesive gels are looser than those in attractive gels, it is easier for adhesive colloids to percolate at the same volume fraction ϕ , i.e., lower gelation time t_g . The above results show that the two models we used lead to two different types of colloidal gels.

Gelation with NS particles. In the presence of NS particles, sticky colloids can still diffuse and aggregate into a percolating gel network, such as Fig. 2 a. Analogous to colloidal gels where ϕ directly controls gelation, the gelation in binary systems depends on the volume fractions of gel colloids ϕ_g and NS particles ϕ_{NS} . Since NS particles do not directly participate in the formation of gel network, we expect them to geometrically confine gelation and compress the free volume V_{free} for sticky

colloids. The reduction in V_{free} then leads to an effective increase in the colloidal volume fraction. If simply consider V_{free} by subtracting the NS particle volume V_{NS} from the total volume V_{tot} , we can then define an effective volume fraction ϕ_{eff} for gel colloids as below:

$$\phi_{eff} \equiv \frac{V_g}{V_{free}} = \frac{V_g}{V_{tot} - V_{NS}} = \frac{\phi_g}{1 - \phi_{NS}}. \quad (3)$$

Though the definition above neglects the exclusion shell around NS particles [36], it has been verified to well capture the gelation diagram with varying attractions [24]. This is probably because as clusters grow and become increasingly large and porous, the cluster-NS interpenetration [37] invalidates the application of exclusion shell.

We first focus on the case of large NS particles with $d_{NS} = 8d$, where d_{NS} and d refer to the sizes of NS particles and gel colloids, respectively. According to Fig. 1 b and Eq. (3), the addition of NS particles is expected to decrease the gelation time t_g . For both models at high ϕ_g ($\phi_g \geq 0.15$ for attractive systems and $\phi_g \geq 0.07$ for adhesive systems), t_g decreases with the volume fraction of NS-particles ϕ_{NS} monotonically, Fig. 2 b. Plotting t_g versus ϕ_{eff} collapses these high- ϕ_g data on a master curve, Fig. 2 c, which converges with the gel data we have shown in Fig. 1 c. In this way, regardless of contact models, the effective volume fraction ϕ_{eff} seems to well characterize the gelation time t_g of sticky-NS composites.

At low ϕ_g , nevertheless, the decrease in t_g becomes progressively slow as ϕ_{NS} increases. In particular, for attractive systems at $\phi_g = 0.07$, the gelation time t_g even increases with the addition of NS particles at high ϕ_{NS} and becomes higher than that of the pure gel, Fig. 2 b (top). This conflicts with our expectation of increasing ϕ_{eff} . Furthermore, plotting t_g versus ϕ_{eff} shows deviation

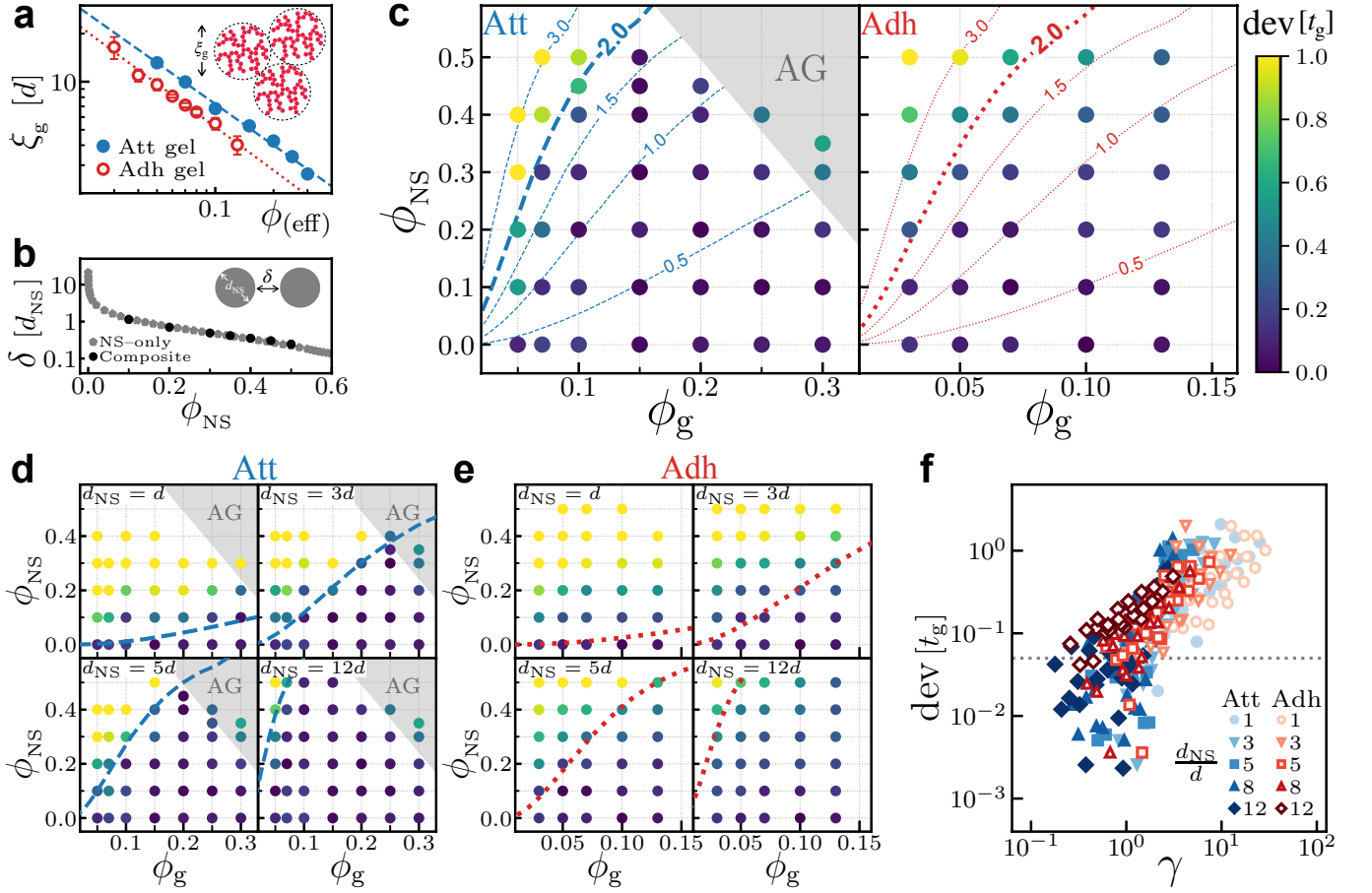


Fig. 3. Interplay between lengthscales affects gelation with NS particles. **a** Characteristic lengthscale ξ_g as a function of volume fraction ϕ in colloidal gels. Dashed and dotted lines are power-law fittings with results shown in Eqs. (4) and (5). **b** Average spacing δ between NS particles as a function of ϕ_{NS} . Gray stars are from individual simulations of only NS particles, while black filled circles are from binary composites with various ϕ_g and d_{NS} . The NS spacing δ is determined through Voronoi analysis in both cases (see the Methods section). **c** ϕ_g - ϕ_{NS} diagrams in attractive (left) and adhesive (right) systems with $d_{NS} = 8d$. Color indicates the value of $\text{dev}[t_g]$. Gray region refers to AG regime with $\phi_{\text{eff}} > 0.4$. Lines refer to the iso- γ lines with values shown on each of them. **d** and **e** are diagrams in attractive systems and adhesive systems with various d_{NS} shown on the upper-left corner of each diagram. Dashed and dotted lines refer to $\gamma = 2$. **f** Plot of $\text{dev}[t_g]$ versus γ , including all the data presented in **c**-**e**. Deviations below the dotted line ($\text{dev}[t_g] = 0.05$) are considered as random error only.

from the master curve, Fig. 2c. While the data collapse at high ϕ_g justifies the definition of ϕ_{eff} , this inconsistency indicates another physics, manifesting at low ϕ_g , that delays the gelation with NS particles.

Lengthscale interplay and diagrams. As previously mentioned, one notable feature of gel-particle composites is the comparable lengthscales. Here we identify two key lengthscales from each constituent and attribute the abnormal deviation from ϕ_{eff} prediction (Fig. 2c) to their interplay. The first lengthscale is the characteristic size ξ of the gel structure derived from structure factor $S(q)$, which evolves over time (Fig. 1c). Since our focus is the gelation time t_g , we measure the structure factor $S(q)$ at $t = t_g$ (Supplementary Note 2) and extract a time-independent lengthscale $\xi_g \equiv \xi(t_g)$. Such lengthscale in general represents the correlation length at gelation

point, Fig. 3a(inset).

For both attractive and adhesive gels, ξ_g decreases with volume fraction ϕ , Fig. 3a. Namely, the more concentrated a system is, the smaller clusters it requires to assemble into percolating network. This is consistent with the gelation at DLCA limit [38]. Power-law fittings on the two sets of data give similar exponents, while the lengthscale in adhesive gels ξ_g^{adh} is a bit lower than that in attractive gels ξ_g^{att} at the same ϕ . Fitting results are as below:

$$\xi_g^{\text{att}} \approx 1.01 \times \phi^{-0.86}, \quad (4)$$

$$\xi_g^{\text{adh}} \approx 0.65 \times \phi^{-0.90}. \quad (5)$$

Note that the above ξ_g refers to the lengthscale in pure colloidal gels and ϕ to the colloid volume fraction. In binary systems, the large NS particles can easily distort

the large scale structure so that the colloid–colloid structure factor $S(q)$ barely exhibits a resolvable peak at low q (Supplementary Fig. 3a). We therefore assume that the ϕ_{eff} scenario also applies to the ξ_g scaling, by simply replacing ϕ with ϕ_{eff} in Eqs. (4) and (5). That is, we use ξ_g in an equivalent pure gel as a proxy for that in a binary composite. By comparing the void distribution [39] in pure gels and composites, we justify such assumption in Supplementary Note 3.

Apart from geometric confinement, NS particles also generate a flexible porous medium [40], in which colloids diffuse and aggregate into a gel network. Such medium is in general characterized by the pore size [20]. Here we use the spacing between NS particles δ to represent the porosity, Fig. 3b (inset). In particular, we simulate a collection of only NS particles at different volume fractions ϕ_{NS} and measure the average interstice δ from Voronoi cell volume (the Methods section). In the unit of d_{NS} , the average spacing δ , diverging at $\phi_{\text{NS}} = 0$, decreases with ϕ_{NS} as shown in Fig. 3b. Though we measure δ in pure NS-particles systems, such quantity in binary mixtures remains almost unchanged at the same ϕ_{NS} (see gray and black scatters in Fig. 3b). Moreover, as gelation proceeds, δ barely varies over time (Supplementary Fig. 5). Thus, δ is time-independent and scales with NS particles’ absolute, rather than relative, volume fraction.

Given other parameters in a binary system fixed, both ξ_g and δ can be *a priori* determined by ϕ_{eff} and ϕ_{NS} , respectively. Then their ratio $\gamma \equiv \xi_g/\delta$ varies as a function of ϕ_g , ϕ_{NS} , and d_{NS}/d . Since the ξ_g -scaling is different in the attractive and adhesive gels, as shown in Eqs. (4) and (5), the lengthscale ratio γ also depends on the specific contact model.

We find that the t_g deviation from the master curve (Fig. 2c) correlates with γ . To quantify the degree of deviation, we use the distance between the average of measured t_g and the predicted t_g^{fit} from power-law fitting, defined as follow:

$$\text{dev}[t_g] \equiv \left| \log t_g - \log t_g^{\text{fit}} \right|, \quad (6)$$

where t_g^{fit} refers to the gelation time calculated by Eq. (1) or (2) but using ϕ_{eff} instead of ϕ . With all the data shown in Fig. 2c, we map out the ϕ_g – ϕ_{NS} diagrams for both gel models at $d_{\text{NS}} = 8d$, Fig. 3c. The quantified deviation $\text{dev}[t_g]$ is represented by the colormap.

For attractive systems, while most data show small $\text{dev}[t_g]$, we observe two regions that present visible deviations in the diagram, Fig. 3c (left). At high ϕ_g and ϕ_{NS} , the effective volume fraction ϕ_{eff} is so high that the system falls in the AG regime with $\phi_{\text{eff}} > 0.4$ (gray). This is consistent with the deviation at high ϕ_{eff} in Fig. 2c, where the measured t_g falls below the power-law fitting (blue dashed line).

Significant deviation also occurs at low ϕ_g and high ϕ_{NS} (upper left corner of the diagram). By drawing the

iso- γ lines, we find that higher γ leads to more prominent deviation $\text{dev}[t_g]$. Namely, when the characteristic size in gel ξ_g far exceeds the spacing δ between NS particles, gelation is greatly hindered by their interplay, which dominates over the effect of ϕ_{eff} .

We use the same method to calculate the ratio γ as well as the deviation $\text{dev}[t_g]$ in adhesive systems and find that this scenario appears to still work, Fig. 3c (right). As the lengthscale ratio γ increases, the deviation becomes significant at low ϕ_g and high ϕ_{NS} . For both systems, visually, the iso- γ line of $\gamma = 2$ demarcates the regions with low and high deviations. This result supports our argument that, as an important factor, the lengthscale interplay primarily affects the gelation process in binary systems at high γ .

The role of lengthscale ratio γ is further verified by varying d_{NS} from d to $12d$ in both gel models, Fig. 3d and e. At the same composition, the lengthscale ratio γ decreases with the NS particle size d_{NS} . For larger NS particles of $d_{\text{NS}} = 12d$, therefore, most data points fall on the master curve when plotting t_g versus ϕ_{eff} (Supplementary Fig. 6), and t_g deviation is greatly suppressed due to the small γ . As d_{NS} decreases, deviation becomes increasingly significant. When the colloids and NS particles have comparable sizes (i.e., $d_{\text{NS}} = d$), almost all data points deviate from the master curve (Supplementary Fig. 6). Raw data of diagrams in Fig. 3d and e can be found in Supplementary Note 5.

Remarkably, the iso- γ line at $\gamma = 2$ demarcates the low- and high-deviation regions in all cases, Fig. 3c–e. The positive correlation between deviation and lengthscale ratio γ is obvious when plotting all the data together, Fig. 3f.

Regardless of the interaction (attractive or adhesive), composition (ϕ_g and ϕ_{NS}), and particle size ratio d_{NS}/d , the lengthscale ratio γ , as well as the effective volume fraction ϕ_{eff} , seems to well characterize the gelation pro-

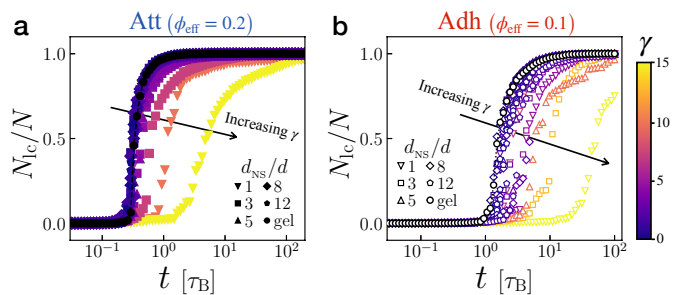


Fig. 4. Lengthscale ratio γ controls cluster growth. **a** Time evolutions of particle fraction in the largest cluster N_{ic}/N of attractive systems with $\phi_{\text{eff}} = 0.2$. **b** Time evolutions of N_{ic}/N in adhesive systems with $\phi_{\text{eff}} = 0.1$. In each plot, data of pure gels ($\phi = \phi_{\text{eff}}$) are shown in black. Detailed compositions are not shown; instead we use γ represented by the color. Arrows indicate increasing γ .

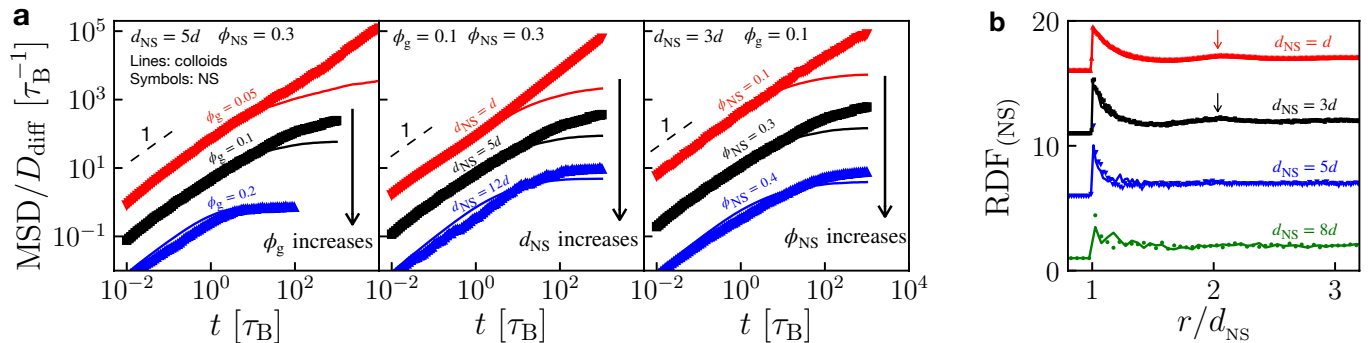


Fig. 5. Behavior of NS particles during gelation. **a** Normalized MSD of colloids (lines) and NS particles (symbols). While varying ϕ_g (left), d_{NS} (middle), and ϕ_{NS} (right) individually, the other two parameters are fixed with values shown on the upper left corner. For better comparison, data in red and black are shifted by 100 and 10 respectively. **b** RDF of NS particles in composites of $\phi_g = 0.1$ and $\phi_{NS} = 0.3$. Visible peaks are highlighted by arrows. Lines and symbols represent data before and after gelation. For better comparison, data of $d_{NS} = d, 3d,$ and $5d$ are shifted by 15, 10, and 5, respectively.

cess in binary mixtures.

Growth of the largest cluster. The deviation from ϕ_{eff} scenario indicates an additional hindering effect at high γ . Such hindering results from the frustration on cluster growth. In particular, we examine the evolutions of particle fraction in the largest cluster N_{lc}/N . For each contact model, we compare systems with different compositions and d_{NS} but the same ϕ_{eff} ($\phi_{eff} = 0.2$ for attraction and $\phi_{eff} = 0.1$ for adhesion), Fig. 4. The value of lengthscale ratio γ is represented by the color. Compared with the pure gel at $\phi = \phi_{eff}$ (black), binary systems with small γ exhibit similar growth while those with large γ show delayed increase in N_{lc}/N . Interestingly, the cluster morphology appears to be barely affected by NS particles regardless of γ (Supplementary Note 6). These results explicitly show how the lengthscale interplay, represented by the unified parameter γ , affects colloidal gelation with NS particles.

Behavior of NS particles. While colloids aggregate into porous network as gelation proceeds, the dynamics of NS particles varies from system to system. At dilute ϕ_g and small d_{NS} , we expect NS particles to be able to diffuse even upon gelation since the pore size of the gel matrix is much larger than the NS particles. As the size of pores shrinks, the NS diffusion starts to be confined until finally ‘locked’ in the matrix cage as soon as a gel network is formed.

To probe the effect of ϕ_g , ϕ_{NS} , and d_{NS} on NS dynamics, we measure the mean squared displacement (MSD) in various composite samples. For ease of comparison between colloids and NS, we normalize MSD by diffusion coefficient D_{diff} for each species of particles. We find that increasing ϕ_g and d_{NS} both lead to the dynamical arrest of NS, which seems to occur simultaneously with that of colloids, Figure 5a (left and middle). This may correspond to the case where NS size exceeds the pore size of the gel matrix, which decreases with ϕ_g as in Supple-

mentary Fig. 4. We also notice that increasing ϕ_{NS} slows down the NS dynamics, Figure 5a (right), probably due to the increasingly crowding surroundings [41].

Through radial distribution function (RDF), we also study the configuration of NS particles in binary composites. Without loss of generality, we use a specific composition of $\phi_g = 0.1$ and $\phi_{NS} = 0.3$ with four different d_{NS} . While a small peak appears at the second-nearest neighbor for small $d_{NS} = d$ and $3d$, such subtle spatial correlation does not present for larger d_{NS} , Figure 5b. We do not identify any sign of crystallization for all cases, and there is little variation in RDF before and after gelation. These results imply that the depletion effect [42, 43] (and the consequent Casimir-like attraction [44]) between NS particles is neglectable.

DISCUSSION

To better illustrate the effect of NS particles, here we consider two limits, Fig. 6. For infinitely-large NS particles ($d_{NS} \rightarrow \infty$), the colloids behave as a continuum which is geometrically confined between solid-wall boundaries, i.e., the surfaces of NS particles. Within the colloidal phase, the real volume fraction is ϕ_{eff} rather than ϕ_g , and the diffusion, as well as aggregation, is purely mediated by the background solvent of viscosity η_f . As the gelation time is proportional to the Brownian time τ_B , we expect the scaling to be $t_g \sim \eta_f(\phi_{eff})^\alpha$, where α refers to an interaction-dependent exponent.

At another limit with $d_{NS} \rightarrow 0$, the NS particles form a continuum background in which sticky colloids are distributed, Fig. 6 (right). In such case, confinement for colloids is absent so that the gelation time scales with the absolute volume fraction ϕ_g rather than the effective one ϕ_{eff} . The continuum background is essentially a hard-sphere suspension, whose viscosity η_{NS} increases with the volume fraction of NS particles [45]. Though such sus-

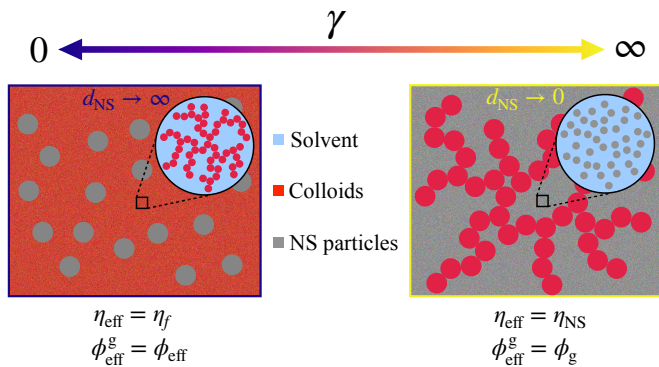


Fig. 6. Schematic illustration of two limit cases in binary systems. Left: $d_{NS} \rightarrow \infty$ ($\gamma \rightarrow 0$). Right: $d_{NS} \rightarrow 0$ ($\gamma \rightarrow \infty$).

pension is not a simple Newtonian fluid of viscosity η_{NS} in general, we may expect so because the situation is close to equilibrium [46]. In this sense, the gelation time then has the form $t_g \sim \eta_{NS}(\phi_g)^\alpha$. For the smallest $d_{NS} = d$ we investigate, the background viscosity η_{NS} increases with ϕ_{NS} roughly in a Krieger–Dougherty manner [47] (Supplementary Note 7).

The above arguments can be generalized by using an effective background viscosity η_{eff} and an effective colloidal volume fraction ϕ_{eff}^g (differing from ϕ_{eff} in Eq. (3)) as follow:

$$t_g \propto \eta_{\text{eff}} \times (\phi_{\text{eff}}^g)^\alpha. \quad (7)$$

The values of η_{eff} and ϕ_{eff}^g at the two limits are shown in Fig. 6. The collapsed gelation time t_g in systems of $d_{NS} = 12d$ validates ϕ_{eff} at large NS particles. For binary systems with $d_{NS} = d$ and the same $\phi_g = 0.1$, the identical structure factor $S(q)$ (Supplementary Fig. 3) and void distribution (Supplementary Fig. 4) suggest that the effective volume fraction ϕ_{eff}^g reduces to ϕ_g at small d_{NS} . Though this conflicts with the previous assumption ($\xi_g - \phi_{\text{eff}}$ scaling), using ϕ_g instead of ϕ_{eff} seems to make little difference in the iso- γ line (Supplementary Note 3).

As d_{NS} decreases from infinity to zero, therefore, we expect transitions in both η_{eff} (from η_f to η_{NS}) and ϕ_{eff}^g (from ϕ_{eff} to ϕ_g). At intermediate d_{NS} , the interpenetration between NS particles and ramified clusters, which weakens the confinement effect and thereby decreases the effective volume fraction ϕ_{eff}^g , becomes possible. Meanwhile, the further aggregation of colloidal clusters with size comparable to the NS spacing ($\gamma \sim 1$) requires the rearrangement of NS particles, which turns on the transition in background viscosity from η_f to η_{NS} . In particular, pinning NS particles during gelation leads to diverging gelation time t_g beyond $\gamma = 2$ (Supplementary Note 8). In this way, the t_g deviation occurs as a result of both the decrease in effective volume fraction ϕ_{eff}^g and the increase of background viscosity η_{eff} .

While the above discussion merely considers d_{NS} , the lengthscale ratio γ , including ϕ_g , ϕ_{NS} , d_{NS} , offers a generic, unified measure in all binary composites. The lengthscale competition then essentially represents a mechanism transition between the two limit cases as shown in Fig. 6. While using global quantities in the expression of γ , we note that local details may also play a secondary role. For example, the lengthscale ratio γ assumes uniform sizes for clusters and NS spacing, which, in practice, both have size distributions (Supplementary Note 4) and irregular morphologies (such as porosity and tortuosity [40, 48]). Meanwhile, as binary systems involve different interactions, the coupling of localized glassy dynamics may also interfere with the formation of gel network [49]. These factors, as well as the others not listed, may more or less affect the gelation process and cannot be fully captured by a sole quantity γ . This is consistent with the scattering of data points in Fig. 3 f.

In summary, we use Langevin dynamics simulations to investigate colloidal gelation with non-sticky particulate fillers. Through extensive exploration in the parameter space, we find that the interplay between two length-scales (ξ_g and δ), represented by their ratio γ , matters in composite gelation. At $\gamma < 2$, the NS particles act as geometric confinement and effectively increase the colloidal concentration in the form of ϕ_{eff} . As γ increases, gelation is progressively hindered as a result of both the decrease in effective concentration and the increasingly-viscous background. Our results not only shed light on industrial formulation and processing, but also open up a new scheme for the tunability in practical gel materials. Though precise prediction is still challenging due to the missing of microscopic details, we successfully capture the generic importance of lengthscale competition in multi-component systems. Our finding will inspire the fundamental understanding and may lead to the efficient development of colloidal composite materials.

METHODS

Simulations. We perform Langevin dynamics simulations on LAMMPS [50]. Under thermostat at $k_B T$, our system contains two species of spherical particles which differ in size and interaction. The first species consists of sticky particles with an average diameter d (bidispersed with $0.87d$ and $1.13d$ to prevent crystallization), while the second species consists of elastic spheres of diameter d_{NS} . To ensure that both colloids and NS particles are diffusive within the relevant time range for gelation process ($\gtrsim 0.1\tau_B$), we set the particle mass proportional to the particle size with the constant damping time $m/3\pi\eta d \ll \tau_B$ (see Supplementary Note 9 for the details). The NS–NS and NS–g interactions are simple elastic repulsions when overlapped, modeled by a modified Hertzian model with

a high modulus $Ed^3 \gg k_B T$. To capture the interaction between sticky colloids, we use the Derjaguin–Muller–Toporov (DMT) contact model [51] with a sufficiently strong attraction $U_{\text{att}} = 20k_B T$. With the same modulus E , the overlap caused by cohesion is small ($\approx 0.01d$) at force balance, ensuring short-ranged attraction. Tangential constraints on sliding, rolling, and twisting (Fig. 1a) are all modeled in a modified Coulomb manner with the same spring constant and friction coefficient μ . Respectively, we set $\mu = 0$ for attraction without constraints and $\mu = 1$ for adhesion with constraints on all three motions.

Our simulation occurs in a cubic box of side length $L = 50d$ with periodic boundaries, which is sufficiently large for bulk condition (Supplementary Fig. 10). In the absence of colloid–colloid attraction, initial configuration is generated through multiple relaxations. We first randomize NS particles and wait for them to relax for $100\tau_B$, and then relax randomly-distributed, non-attractive colloids with pinned NS particles for another $100\tau_B$. Upon equilibrium, we unpin NS particles and allow the bulk system to relax shortly for $10\tau_B$. The initial state generated by such pre-relaxing protocol exhibits no overlapping and no visible aggregation caused by depletion forces. We find little dependence on the pre-relaxing duration (Supplementary Fig. 11), suggesting the robustness of our results.

Starting from a homogeneous random configuration, each system evolves up to $10^4\tau_B$. We run each simulation for at least three times, with the data points and error bars shown in this work representing the average and standard deviation, respectively. Visualization and part of data analysis are carried out using OVITO [52]

Determining gelation time A robust criterion for gelation is crucial to accurately determine the gelation time t_g . The experimental convention views the liquid-to-solid transition, typically characterized by oscillatory rheology [53], as the gelation point. Inspired by the Maxwell criteria for stability [29], recent work, including both simulation [24] and experiment [31], correlates the evolution of clusters of isostatic particles (contact number $N \geq N_c$) with colloidal gelation, and confirms the validity of such structural indicator by comparison with macroscopic rheology.

In this work, we define the gelation time t_g as the time required for the isostaticity percolation. As Fig. 1b shows, we first extract all isostatic particles with $N \geq N_c$ (Table. 1 in [28]) and then examine their connectivity. Gelation is determined if there exist clusters percolating through periodic boundaries in all three directions (x , y , and z). Recent work correlates rigidity percolation with gelation boundary [54]. For adhesive systems, our method (isostatic percolation with $N_c^{\text{adh}} = 2$) gives the same result as rigidity percolation, since each pair constitutes a minimal rigid cluster. Yet this may not hold for attractive contacts with no tangential constraints, where

3D rigidity analysis is challenging [31] (and beyond the scope of this work). Therefore, we consistently apply the isostaticity method for attractive systems with $N_c^{\text{att}} = 6$.

Voronoi analysis and NS-particle spacing To measure the average spacing between NS particles δ , we perform simulations of only NS particles at different volume fractions ϕ_{NS} . Upon Brownian relaxation, Voronoi analysis is performed and the spacing between each pair of particles δ_i is estimated as follow:

$$\delta_i = 2 \times \left(\frac{3V_{\text{cell},i}}{4\pi} \right)^{1/3} - d_{\text{NS}}, \quad (8)$$

where $V_{\text{cell},i}$ refers to the volume of Voronoi cell of i -th particle. Here we assume isotropic distribution and regard each Voronoi polyhedron as an equivalent sphere. Then the average spacing $\delta = \langle \delta_i \rangle$. The distribution of δ_i can be found in Supplementary Fig 5.

DATA AVAILABILITY

The data generated in this study are provided in the Supplementary Information/Source Data file.

CODE AVAILABILITY

The codes of the computer simulations are available from the corresponding authors upon reasonable request.

* jiangyujie@ucas.ac.cn

† seto@ucas.ac.cn

- [1] Lekkerkerker, H. N. W., Poon, W. C.-K., Pusey, P. N., Stroobants, A. & Warren, P. B. Phase behaviour of colloid + polymer mixtures. *Europhys. Lett.* **20**, 559 (1992).
- [2] Poon, W. C. K., Pirie, A. D. & Pusey, P. N. Gelation in colloid–polymer mixtures. *Faraday Discuss.* **101**, 65–76 (1995).
- [3] Bonn, D. & Denn, M. M. Yield stress fluids slowly yield to analysis. *Science* **324**, 1401–1402 (2009).
- [4] Bonn, D., Denn, M. M., Berthier, L., Divoux, T. & Manneville, S. Yield stress materials in soft condensed matter. *Rev. Mod. Phys.* **89**, 035005 (2017).
- [5] Joshi, Y. M. Dynamics of colloidal glasses and gels. *Annu. Rev. Chem. Biomol. Eng.* **5**, 181–202 (2014).
- [6] Harich, R. *et al.* Gravitational collapse of depletion-induced colloidal gels. *Soft Matter* **12**, 4300–4308 (2016).
- [7] Rouwhorst, J., Ness, C., Stoyanov, S., Zaccone, A. & Schall, P. Nonequilibrium continuous phase transition in colloidal gelation with short-range attraction. *Nat. Commun.* **11**, 3558 (2020).
- [8] Laurati, M., Egelhaaf, S. U. & Petekidis, G. Nonlinear rheology of colloidal gels with intermediate volume fraction. *J. Rheol.* **55**, 673–706 (2011).

- [9] Cates, M. E., Fuchs, M., Kroy, K., Poon, W. C. K. & Puertas, A. M. Theory and simulation of gelation, arrest and yielding in attracting colloids. *J. Phys. Condens. Matter* **16**, S4861 (2004).
- [10] Ferreiro-Córdova, C., Del Gado, E., Foffi, G. & Bouzid, M. Multi-component colloidal gels: interplay between structure and mechanical properties. *Soft Matter* **16**, 4414–4421 (2020).
- [11] Jia, D., Hollingsworth, J. V., Zhou, Z., Cheng, H. & Han, C. C. Coupling of gelation and glass transition in a biphasic colloidal mixture—from gel-to-defective gel-to-glass. *Soft Matter* **11**, 8818–8826 (2015).
- [12] Daneshfar, Z., Goharpey, F. & Foudazi, R. Depletion-induced interaction in concentrated bimodal suspensions of nanosilica in poly(ethylene glycol). *Rheol. Acta* **58**, 97–107 (2019).
- [13] Sikorski, M., Sandy, A. R. & Narayanan, S. Depletion-induced structure and dynamics in bimodal colloidal suspensions. *Phys. Rev. Lett.* **106**, 188301 (2011).
- [14] Chang, C. & Powell, R. L. Effect of particle size distributions on the rheology of concentrated bimodal suspensions. *J. Rheol.* **38**, 85–98 (1994).
- [15] Jamali, S., Yamanoi, M. & Maia, J. Bridging the gap between microstructure and macroscopic behavior of monodisperse and bimodal colloidal suspensions. *Soft Matter* **9**, 1506–1515 (2013).
- [16] Muhammed Shameem, M., Sasikanth, S., Annamalai, R. & Ganapathi Raman, R. A brief review on polymer nanocomposites and its applications. *Mater. Today: Proc.* **45**, 2536–2539 (2021).
- [17] Ferreiro-Córdova, C. *et al.* Stiffening colloidal gels by solid inclusions. *Soft Matter* **18**, 2842–2850 (2022).
- [18] Mahaut, F., Chateau, X., Coussot, P. & Ovarlez, G. Yield stress and elastic modulus of suspensions of non-colloidal particles in yield stress fluids. *J. Rheol.* **52**, 287–313 (2008).
- [19] Vu, T.-S., Ovarlez, G. & Chateau, X. Macroscopic behavior of bidisperse suspensions of noncolloidal particles in yield stress fluids. *J. Rheol.* **54**, 815–833 (2010).
- [20] Sorichetti, V., Hugouvieux, V. & Kob, W. Structure and dynamics of a polymer–nanoparticle composite: Effect of nanoparticle size and volume fraction. *Macromolecules* **51**, 5375–5391 (2018).
- [21] Mohraz, A., Weeks, E. R. & Lewis, J. A. Structure and dynamics of biphasic colloidal mixtures. *Phys. Rev. E* **77**, 060403 (2008).
- [22] Harden, J. L. *et al.* Enhanced gel formation in binary mixtures of nanocolloids with short-range attraction. *J. Chem. Phys.* **148**, 044902 (2018).
- [23] Jiang, Y., Makino, S., Royer, J. R. & Poon, W. C. K. Flow-switched bistability in a colloidal gel with non-brownian grains. *Phys. Rev. Lett.* **128**, 248002 (2022).
- [24] Li, Y., Royer, J. R., Sun, J. & Ness, C. Impact of granular inclusions on the phase behavior of colloidal gels. *Soft Matter* **19**, 1342–1347 (2023).
- [25] Zaccarelli, E. Colloidal gels: equilibrium and non-equilibrium routes. *J. Phys. Condens. Matter* **19**, 323101 (2007).
- [26] Richards, J. A. *et al.* The role of friction in the yielding of adhesive non-Brownian suspensions. *J. Rheol.* **64**, 405–412 (2020).
- [27] Pantina, J. P. & Furst, E. M. Elasticity and critical bending moment of model colloidal aggregates. *Phys. Rev. Lett.* **94**, 138301 (2005).
- [28] Santos, A. P. *et al.* Granular packings with sliding, rolling, and twisting friction. *Phys. Rev. E* **102**, 032903 (2020).
- [29] Maxwell, J. C. On the calculation of the equilibrium and stiffness of frames. *Lond. Edinb. Dublin Phil. Mag.* **27**, 294–299 (1864).
- [30] Liu, W., Jin, Y., Chen, S., Makse, H. A. & Li, S. Equation of state for random sphere packings with arbitrary adhesion and friction. *Soft Matter* **13**, 421–427 (2017).
- [31] Tsurusawa, H., Leocmach, M., Russo, J. & Tanaka, H. Direct link between mechanical stability in gels and percolation of isostatic particles. *Sci. Adv.* **5**, eaav6090 (2019).
- [32] Zaccone, A., Crassous, J. J. & Ballauff, M. Colloidal gelation with variable attraction energy. *J. Chem. Phys.* **138**, 104908 (2013).
- [33] Trompette, J. & Meireles, M. Ion-specific effect on the gelation kinetics of concentrated colloidal silica suspensions. *J. Colloid Interface Sci.* **263**, 522–527 (2003).
- [34] Innocenzi, P. *Measuring the Sol-to-Gel Transition*, 51–61 (Springer International Publishing, Cham, 2016).
- [35] Lattuada, M., Wu, H., Hasmy, A. & Morbidelli, M. Estimation of fractal dimension in colloidal gels. *Langmuir* **19**, 6312–6316 (2003).
- [36] Oversteegen, S. M. & Roth, R. General methods for free-volume theory. *J. Chem. Phys.* **122**, 214502 (2005).
- [37] Dagès, N. *et al.* Interpenetration of fractal clusters drives elasticity in colloidal gels formed upon flow cessation. *Soft Matter* **18**, 6645–6659 (2022).
- [38] Poon, W. & Haw, M. Mesoscopic structure formation in colloidal aggregation and gelation. *Adv. Colloid Interface Sci.* **73**, 71–126 (1997).
- [39] Koumakis, N. *et al.* Tuning colloidal gels by shear. *Soft Matter* **11**, 4640–4648 (2015).
- [40] Peppin, S. S. L. Theory of tracer diffusion in concentrated hard-sphere suspensions. *J. Fluid Mech.* **870**, 1105–1126 (2019).
- [41] Brady, J. F. The long-time self-diffusivity in concentrated colloidal dispersions. *J. Fluid Mech.* **272**, 109–134 (1994).
- [42] Royall, C. P., Louis, A. A. & Tanaka, H. Measuring colloidal interactions with confocal microscopy. *J. Chem. Phys.* **127**, 044507 (2007).
- [43] Roth, R., Evans, R. & Dietrich, S. Depletion potential in hard-sphere mixtures: Theory and applications. *Phys. Rev. E* **62**, 5360–5377 (2000).
- [44] Gnan, N., Zaccarelli, E. & Sciortino, F. Casimir-like forces at the percolation transition. *Nat. Commun.* **5**, 3267 (2014).
- [45] Mewis, J. & Wagner, N. J. *Colloidal Suspension Rheology*. Cambridge Series in Chemical Engineering (Cambridge University Press, 2011).
- [46] Mari, R., Seto, R., Morris, J. F. & Denn, M. M. Shear thickening, frictionless and frictional rheologies in non-brownian suspensions. *J. Rheol.* **58**, 1693–1724 (2014).
- [47] Krieger, I. M. & Dougherty, T. J. A mechanism for non-newtonian flow in suspensions of rigid spheres. *Trans. Soc. Rheol.* **3**, 137–152 (1959).
- [48] Gelb, L. D., Graham, A. L., Mertz, A. M. & Koenig, P. H. On the permeability of colloidal gels. *Phys. Fluids* **31**, 021210 (2019).
- [49] Pham, K. N. *et al.* Multiple glassy states in a simple model system. *Science* **296**, 104–106 (2002).
- [50] Thompson, A. P. *et al.* LAMMPS - a flexible simulation tool for particle-based materials modeling at the atomic,

- meso, and continuum scales. *Comput. Phys. Commun.* **271**, 108171 (2022).
- [51] Derjaguin, B., Muller, V. & Toporov, Y. Effect of contact deformations on the adhesion of particles. *J. Colloid Interface Sci.* **53**, 314–326 (1975).
- [52] Stukowski, A. Visualization and analysis of atomistic simulation data with ovito—the open visualization tool. *Model. Simul. Mater. Sci. Eng.* **18**, 015012 (2009).
- [53] Ishida, H. & Agag, T. *Handbook of Benzoxazine Resins* (Elsevier, Amsterdam, 2011).
- [54] Zhang, S. *et al.* Correlated rigidity percolation and colloidal gels. *Phys. Rev. Lett.* **123**, 058001 (2019).

ACKNOWLEDGMENTS

R.S. acknowledge funding from Wenzhou Institute, University of Chinese Academy of Sciences (WIU-

CASQD2020002), National Natural Science Foundation of China (12174390, 12150610463). Y.J. acknowledge funding from China Postdoctoral Science Foundation (2022M723114). We thank PostDoctoral Association (PDA) and Journal Club (JC) in Wenzhou Institute for fruitful discussions.

AUTHOR CONTRIBUTIONS

Y.J. conceive the research and carry out the simulation. Y.J. and R.S. analyze the data and write the manuscript.

COMPETING INTERESTS

The authors declare no competing interests.